Eur. Phys. J. A **29**, 235–244 (2006)
DOI 10.1140/epja/i2006-10081-1

THE EUROPEAN PHYSICAL JOURNAL A

Spectral patterns in the nonstrange-baryon spectrum

P. González[1], J. Vijande[1,2], A. Valcarce[2,a], and H. Garcilazo[3]

[1] Departamento de Física Teórica and IFIC, Universidad de Valencia - CSIC, E-46100 Burjassot, Valencia, Spain
[2] Grupo de Física Nuclear and IUFFyM, Universidad de Salamanca, E-37008 Salamanca, Spain
[3] Escuela Superior de Física y Matemáticas, Instituto Politécnico Nacional, Edificio 9, 07738 México D.F., Mexico

Received: 13 June 2006 /
Published online: 8 September 2006 –
Communicated by V. Vento

Abstract. We extract, from a quark model potential that reproduces the number and ordering of nonstrange baryonic resonances up to 2.3 GeV, the quantum numbers for the dominant configurations in the ground and first nonradial excited states. From the pattern of quantum numbers we identify, from data, spectral regularities that allow us to predict the expected high-spin low-lying spectrum from 2.3 to 3.0 GeV. $N-\Delta$ degeneracies and N parity doublets showing up can be interpreted in terms of a simple dynamics.

PACS. 12.39.Jh Nonrelativistic quark model – 14.20.-c Baryons (including antiparticles) – 14.20.Gk Baryon resonances with $S = 0$

1 Introduction

There has been much interest during the last years in the high-energy part of the hadronic spectrum. The aim is to get a better understanding of the dynamics involved, in particular the confinement mechanism in hadrons. On the theoretical side some progress has been made. On the one hand, unquenched lattice QCD points out a string breaking in the static potential between two quarks [1,2] what should be properly incorporated in the phenomenological description of the high-energy hadronic spectrum through the coupling to open decay channels. On the other hand, the idea of a parity multiplet classification scheme at high excitation energies as due to chiral symmetry has been suggested [3] and recently put in question [4]. On the experimental side, the lack of precise and complete data prevents, at the current moment, to establish in a clear-cut way a classification scheme for the highly excited hadron spectrum. Hence, it may be appropriate to try to extract, from a simple dynamical quark model calculation and its comparison to data, some spectral patterns. To this purpose we shall consider the light-baryon spectrum for which an extensive collection of data including high-spin state masses, though not very precise in some cases, exists.

We shall use a nonrelativistic quark potential model. The application of such approach for high excited states deserves some comments since the quarks inside the baryons may be ultra-relativistic, $q\overline{q}$ pair creation out of the vacuum becomes more and more relevant as the number of open decay channels increases, etc. As is well known these shortcomings, always implicit in the application of the naive quark model, do not invalidate its usefulness to provide information about the pattern of the quantum numbers of the baryon states. To get an unambiguous assignment of quantum numbers one should require the model to generate, inasmuch as possible, the correct number and ordering of the well-established experimental states. Different dynamical models providing accurate descriptions of the low-energy baryon spectrum have been proposed [5]. Most of them rely on nonlimited (usually linearly dependent on the interquark distance) confinement interactions. As a consequence, above 1.9 GeV, there are many more predicted states than observed resonances. This *missing state* problem can be solved by ascribing experimental resonances (in the πN partial-wave analysis) to predicted states with a significant coupling to the πN formation channel [6].

Alternatively, the missing state problem can be obviated by using a quark-quark screened potential as shown in ref. [7], where a correct prediction of the number and ordering of the known N and Δ resonances, up to 2.3 GeV mass, is obtained. This points out to screening as an effective manner to give somewhat account of the coupling to πN channels (lattice calculations have unveiled the close relation between screening and the opening of decay channels). Such interpretation is supported by the fact that the quantum numbers of the dominant configurations (for the ground and first excited states of given J) coming out from a screened potential (containing only confinement and a residual one-gluon exchange (OGE) interaction) are in perfect agreement with the ones ascribed to

[a] e-mail: valcarce@usal.es

data from refined non-screened models through the coupling analysis, as we have explicitly checked for $J \leq 7/2$ (see ref. [6] for the identification of the available dominant nonscreened configurations).

Though one cannot expect, from the minimal screened dynamics employed, to get an accurate description of the values of the baryon masses, it is clear its convenience to provide an unambiguous assignment of quantum numbers to baryon states beyond the sometimes *ad hoc* arguments that have to be used in nonscreened models to identify the experimental resonances when the πN coupling strengths have similar values for different predicted candidates.

However, the smooth screening parametrization employed in ref. [7], suggested from old lattice data [8], does not keep a direct relation to more recent lattice results [2] pointing out a rather abrupt string breaking (rehadronization) transition in the potential. Here, we deepen this relation. To this purpose the comparison with a sharply saturated potential is useful. We analyze the resulting baryon spectrum for both (smooth and sharp) models and compare the resulting dominant configurations for any angular momentum. We generate patterns of quantum numbers and associate to them spectral regularities observed in the data. From them we are able to make purely phenomenological detailed predictions for resonances above 2.3 GeV, many of them not experimentally identified yet. From data and our predictions we identify $N-\Delta$ degeneracies and N parity series that have a dynamical understanding within our quark model framework.

These contents are organized as follows. In sect. 2 we introduce and discuss the models used and their results for the nonstrange baryon spectra. The analysis of the dominant contributions and the subsequent derivation of spectral patterns is carried out in sect. 3. Finally, in sect. 4 we summarize our main findings.

2 The model

In the absence of sea quarks lattice QCD predicts the static heavy-quark–heavy-antiquark ($Q\overline{Q}$) interacting potential to rise linearly with the quark-antiquark distance [1]. Unquenched (valence + sea quarks) lattice calculations point out the existence of string breaking in QCD. This is, the static $Q\overline{Q}$ force becomes screened by intermediate light $q\overline{q}$ pairs, so that when the $Q\overline{Q}$ distance exceeds a critical value (the breaking distance) the $Q\overline{Q}$ potential saturates to a constant (saturation energy). In the 1980s a smooth screened potential was proposed to parametrize this effect [8]. In the last decade such a parametrization has been implemented in valence quark models in an attempt to examine the consequences of string breaking in heavy quarkonia as well as in the nonstrange-baryon spectra [7,9–12].

The simplest quark-quark screened potential, containing confinement and one-gluon exchange terms, reads (the factor 1/2 has been explicitly written since it reflects the difference between the quark-quark and quark-antiquark interactions):

$$V(r_{ij}) = \frac{1}{2}\left[\overline{\sigma} r_{ij} - \frac{\overline{\kappa}}{r_{ij}} + \frac{\hbar^2 \overline{\kappa_\sigma}}{m_i m_j c^2}\frac{e^{-r_{ij}/\overline{r_0}}}{\overline{r_0}^2 r_{ij}}(\vec{\sigma_i}\cdot\vec{\sigma_j})\right] \times \left(\frac{1-e^{-\mu\, r_{ij}}}{\mu\, r_{ij}}\right) + \frac{\overline{M_0}}{3}\,, \quad (1)$$

where r_{ij} is the interquark distance, $m_{i,j}$ the masses of the constituent quarks, $\vec{\sigma}_{i,j}$ the spin Pauli operators, and $\overline{M_0}$ is a constant to fix the ground-state nucleon mass. The screening multiplicative factor appears between parenthesis on the right-hand side. μ, the screening parameter, is the inverse of the saturation distance and its effective value is fitted together with the other parameters, $\overline{\sigma}$, $\overline{\kappa}$, and $\overline{\kappa_\sigma}$, to the spectrum ($\mu^{-1} \simeq 1.4$ fm for heavy quarkonia and $\mu^{-1} \simeq 1$ fm for nonstrange baryons) [7,12].

In the heavy-meson sector a good description of bottomonium (the only truly nonrelativistic quarkonia) is obtained. For nonstrange baryons the model predicts quite approximately the number and ordering of the experimental states up to a mass of 2.3 GeV. For the sake of completeness, we show improved results (with more channels entering in the description) from ref. [7] in figs. 1 and 2. Let us note that the ordering discrepancies, related to the relative position of the first excited states of positive and negative parity in N and Δ, are endemic in this kind of quark model treatments; the number discrepancy related to the presence of two, instead of one, excited states for $N(3/2^+)$ and $N(5/2^+)$ might have to do with the presence

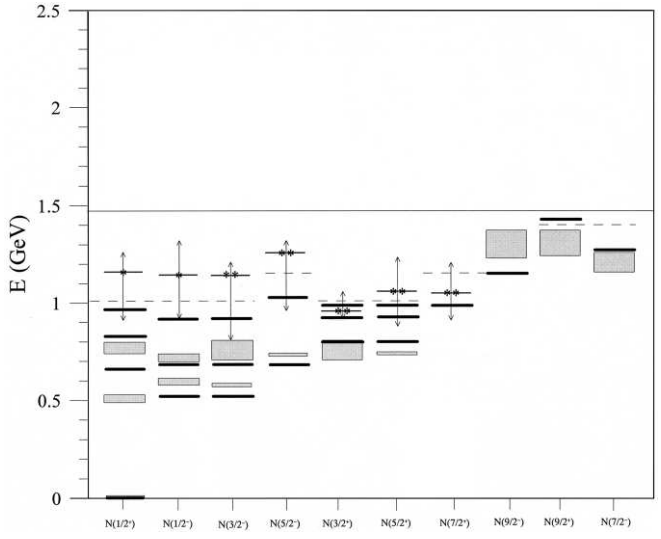

Fig. 1. Relative energy nucleon spectrum for the screened potential of eq. (1) with the parameters of ref. [7]. The thick solid lines represent our results. The shaded region, whose size stands for the experimental uncertainty, represents the experimental data for those states cataloged as (∗∗∗) or (∗∗∗∗) states in the Particle Data Book [13]. Experimental data cataloged as (∗) or (∗∗) states are shown by short thin solid lines with stars over them and by vertical lines with arrows standing for the experimental uncertainties. Finally, we show by a dashed line the $1q$ ionization threshold and by a long thin solid line the total threshold.

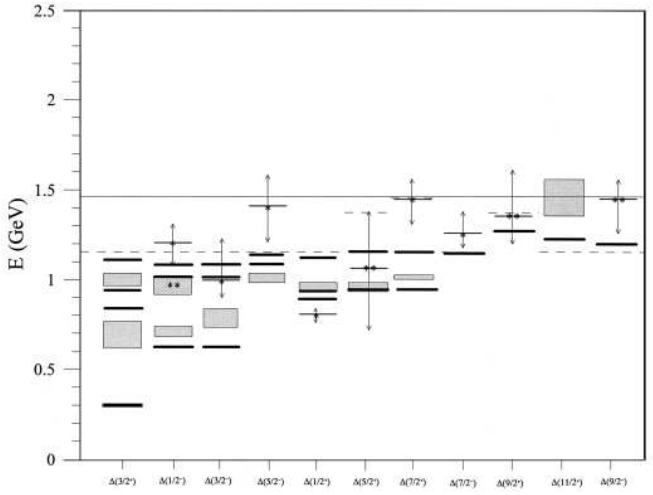

Fig. 2. The same as fig. 1 for Δ states.

of two degenerate excitations at the experimental level of precision.

More recent lattice QCD calculations [2] show that the $Q\overline{Q}$ potential saturates sharply for a breaking distance of the order of 1.25 fm corresponding to a saturation energy of about twice the B-meson ($Q\overline{q}$) mass, indicating that the formation of two heavy-light subsystems $(B, \overline{B})$ is energetically favored. This information has been implemented in a quark model scheme [14] showing that, as a consequence of coupled channels above the physical thresholds (corresponding to the opening of decay channels), the description becomes progressively less accurate high in the spectrum. Moreover, the mixing with the continuum can also modify the short-range part of the interaction. Nonetheless, an effective (renormalized) nonscreened potential continues being useful up to energies not too far above the lowest physical threshold.

These results provide some understanding of the successful application of the smooth screened potential of eq. (1) in refs. [7] and [12]. For bottomonium, the maximum value of the potential, $\overline{\sigma}/\mu = 2070\,\mathrm{MeV}$ (the b mass has been chosen so that the constant term in the potential vanishes), translates into an upper limit for the energy of bound states of $2m_b+\overline{\sigma}/\mu = 11400\,\mathrm{MeV}$ [12], far above the lowest physical threshold, assuring that the potential does not differ much from a nonscreened one (corresponding to eq. (1) without the multiplicative screening factor) for the experimentally known states. As a matter of fact, one can alternatively use for bottomonium a (linear + Coulomb) potential sharply saturated at an energy just above the highest resonance experimentally known,

$$V(r_{ij}) = \begin{cases} \sigma r_{ij} - \kappa/r_{ij}\,, & r_{ij} < r_{sat}\,, \\ \sigma r_{sat} - \kappa/r_{sat}\,, & r_{ij} \geq r_{sat}\,, \end{cases} \qquad (2)$$

and maintain the quality of the description [15]. Let us note that this is the closest approach one can do to a nonscreened potential if one wants to extend its use high in energy since the sharp saturation prevents a proliferation of predicted states without experimental counterpart.

Table 1. Quark model parameters.

$m_u = m_d$ (MeV)	337
r_0 (fm)	0.495
r_{sat} (fm)	2.12
κ (MeV fm)	10.0
κ_σ (MeV fm)	120.0
σ (MeV fm^{-1})	976.56
M_0 (MeV)	−1726.78

We should then keep in mind that the fitted saturation distance, r_{sat}, should not be identified with the lattice breaking distance at the physical threshold but as an effective parameter to establish the limit of applicability of the model (in fact its fitted value, 1.76 fm, differs a 30% of the breaking value 1.25 fm).

In the nonstrange-baryon case, the maximum possible value of the energy of bound states for the screened potential in ref. [7], $3m_q + \overline{M_0} + 3\overline{\sigma}/(2\mu) \simeq 2.4\,\mathrm{GeV}$, very close to the highest experimental resonance catalogued as four stars by the Particle Data Group (PDG) [13], $\Delta(11/2^+)$ at 2420 MeV, reflects the difficulty of pushing the applicability limit of the model beyond this energy. It is interesting to make again a comparison with a sharply saturated potential of the form:

$$V(r_{ij}) = \begin{cases} V_{sr}(r_{ij})\,, & r_{ij} < r_{sat}\,, \\ V_{sr}(r_{sat})\,, & r_{ij} \geq r_{sat}\,, \end{cases} \qquad (3)$$

where

$$V_{sr}(r_{ij}) = \frac{1}{2}\left[\sigma r_{ij} - \frac{\kappa}{r_{ij}} + \frac{\hbar^2\kappa_\sigma}{m_i m_j c^2}\frac{e^{-r_{ij}/r_0}}{r_0^2 r_{ij}}(\vec{\sigma_i}\cdot\vec{\sigma_j})\right] + \frac{M_0}{3}\,, \qquad (4)$$

whose parameters, given in table 1, are fitted to get a global description of the nonstrange-baryon spectrum while choosing r_{sat} to keep the same value for the saturation energy $3m_q + M_0 + 3\sigma r_{sat}/2 \simeq 2.4\,\mathrm{GeV}$ (splitting energy of the three pairs of quarks). We draw this sharp potential and the smooth one in fig. 3. The calculation of the spectrum proceeds exactly in the same manner as in ref. [7], to which we refer for technical details. Let us only remind for the moment that two different calculational methods, hyperspherical harmonic expansion (HH) and Faddeev, are employed and that convergence of the results is required. The resulting spectrum is shown in figs. 4 and 5.

It is worth to remark that the presence, in the three-body problem, of two-body thresholds (for only one quark to be released, values quoted in table 2), apart from the absolute three-body one (saturation energy), may represent further constraints in the applicability limit of the model to any particular channel. As in ref. [7] we have also included the predicted states close above the thresholds.

The comparison of figs. 4 and 5 with figs. 1 and 2 shows that the sharp potential tends quite generally to push upward the highest-energy states. However, as we can check there is little difference concerning the number and ordering of states. Both models give them quite reasonably. In

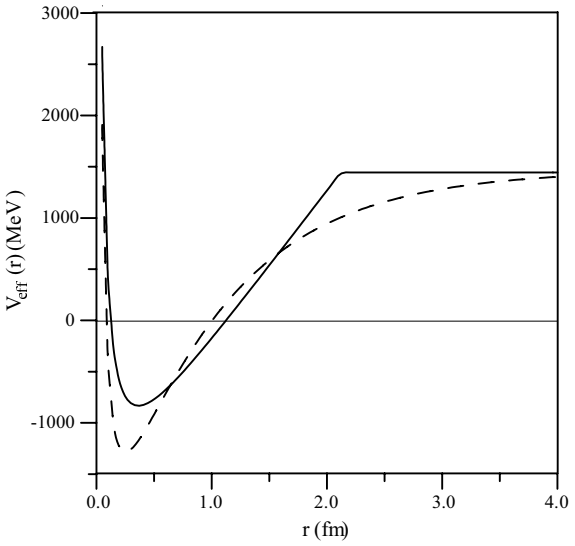

Fig. 3. Effective interaction, $3\,V(r_{ij}) - E_N$, for the potentials $V(r_{ij})$ of eq. (1), dashed line, and eq. (3), solid line, for a two-particle spin-1 state. E_N stands for the eigenvalue of the nucleon ground state with the corresponding potential.

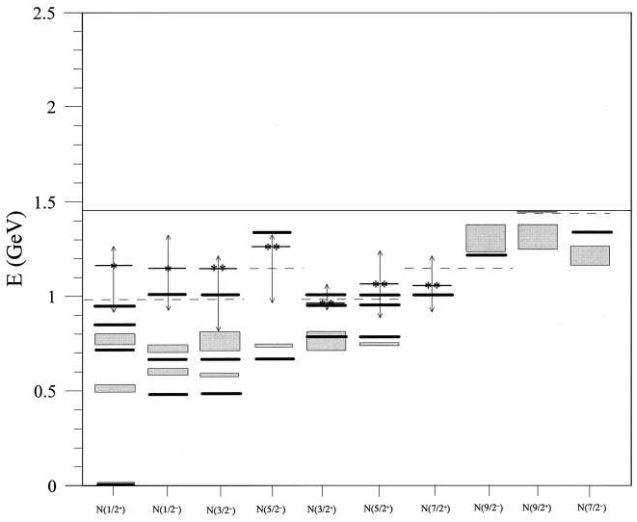

Fig. 4. The same as fig. 1 for the screened potential of eq. (3) with the parameters of table 1.

other words, the screened potential is quite similar, concerning these results, to the closest physical approach to a nonscreened potential, represented by the sharp interaction, that takes effectively into account the effect of the baryon decay to open channels in order to select the observed resonances.

Let us notice further that the sharp-potential model permits to establish in a direct way the subtle connection between the lowest two-body (2bt) and three-body thresholds (3bt): if the 3bt is increased (changing for example r_{sat}) and one refits the spin-spin and Coulomb terms to recover the experimental $\Delta - N$ mass difference, the 2bt is increased, almost linearly, in correspondence. Otherwise said, the 2bt (3bt) plus the $\Delta - N$ mass difference fixes the

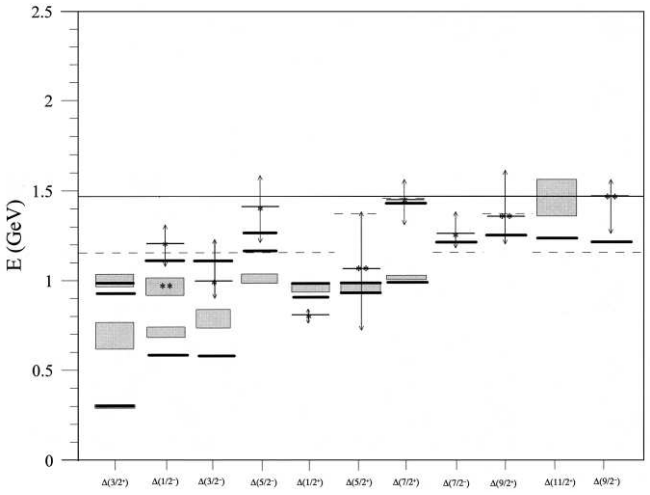

Fig. 5. The same as fig. 4 for Δ states.

Table 2. One-quark ionization thresholds. We give the energy above the nucleon ground-state mass. ℓ is the orbital angular momentum of a pair of quarks, s its relative spin and t its isospin.

(ℓ, s, t)	E (MeV)
$(0, 0, 0)$	984.10
$(0, 1, 1)$	1143.33
$(1, 0, 1)$	1384.15
$(1, 1, 0)$	1416.48

3bt (2bt). This is a realization of the idea that the mixing with the continuum (at least partially contained in the effective thresholds) affects the whole (in particular the short) range of the interaction. Moreover, as the lowest 2bt corresponds to the lowest angular-momentum state, the experimental presence of a well-established high-energy low-angular momentum state can be used as a lower bound to fix the lowest 2bt. Then this fixing procedure determines the maximum energy at which a higher angular-momentum state can be predicted within the range of applicability of the model (a fine tune of this process has been carried out to get the spectrum).

3 Spectral patterns

As shown in figs. 1, 2, 4 and 5, the predicted nonstrange-baryon spectra are quite analogous despite the difference between the two potentials. Furthermore, the dominant configurations entering any J^P ground state and its first nonradial excitation are exactly the same for both potentials (this is not the case for higher excitations as discussed below) giving for them similar quantitative values that differ at most a 13% from data (within the experimental uncertainties). Hence it makes sense to proceed, from our dynamical models, to a quantum number assignement for these states. From the resulting patterns and from the experimental values of the masses of the known resonances we shall make predictions for higher-energy states and we

shall justify (as implied by our dynamical model) approximate degeneracies and the partial appearance of approximate parity doublets.

3.1 J^P ground states

To express the spatial part of the dominant J^P ground-state configurations we shall use the hyperspherical harmonic notation, *i.e.*, the quantum numbers $(K, L(\ell,\lambda), Symmetry)$. The so-called great orbital, K, defines the parity of the state, $P=(-)^K$, and its centrifugal barrier energy, $\frac{\mathcal{L}(\mathcal{L}+1)}{2m\langle\rho^2\rangle}$ ($\mathcal{L}=K+\frac{3}{2}$, ρ: hyperrradius). ℓ is the orbital angular momentum of a pair of quarks, λ stands for the orbital angular momentum of the third quark with respect to the center of mass of this pair and L ($\vec{L}=\vec{\ell}+\vec{\lambda}$) is the total orbital angular momentum. Alternatively, one can write the parity as $P=(-)^{\ell+\lambda}$, since $K-\ell-\lambda=$ even ≥ 0 is always satisfied. *Symmetry* specifies the spatial symmetry ([3] : symmetric, [21] : mixed, [111] : antisymmetric) which combines to the spin, S, and isospin, T, symmetries ($S,T=3/2$: symmetric; $S,T=1/2$: mixed) to have a symmetric wave function (the color part is antisymmetric). More precisely, $T=1/2$ for N and $T=3/2$ for Δ, hence the spatial-spin wave function must be mixed for N and symmetric for Δ.

It is convenient to group the ground states corresponding to the same dominant configuration in our model as done in tables 3 and 4 (note that above 2.4 GeV the dominant configurations correspond to an extrapolation of the pattern).

As a first general rule we have

$$P=(-)^L\,, \tag{5}$$

for the dominant configuration in J^P ground states. This comes, except for $\Delta(1/2^+)$, from $(\ell=0,\lambda)$ and/or $(\ell,\lambda=0)$ components for which $L=\ell+\lambda$. For $\Delta(1/2^+)$ one has $L=0$ with $\ell=1=\lambda$ instead of $\ell=0=\lambda$ due to the more attractive spin-spin interaction.

The second general rule, of general validity for states with $J\geq 5/2$, can be formulated as follows:

$$J\geq 5/2\ :\quad J=L+S\quad\text{with}\quad L\quad\text{minimal}\,. \tag{6}$$

For states with lower total angular momentum such rule is not always verified. In particular, it is not fulfilled by the $N(3/2^+)$ and $N,\Delta(1/2^-)$. For $N(3/2^+)$ the rule would prescribe $(L=0,S=3/2)$, hence spin symmetric and consequently spatially mixed. Dynamically, a spatially symmetric $(L=2,S=1/2)$ configuration, with a spin-spin attractive contribution, is favoured. For $N,\Delta(1/2^-)$, according to the parity expression, $L=$ odd and eq. (6) cannot be satisfied. In all these exceptional cases $J=L-S$, with S minimal, provides the minimum energy. Otherwise said, at the level of dominant configurations, the $N(3/2^+)$ and the $N(5/2^+)$ are degenerate as well as the $N,\Delta(1/2^-)$ and the $N,\Delta(3/2^-)$, respectively. These degeneracies are quite well satisfied by data, see tables 3 and 4.

These two rules, complemented with the prescription of having the minimum value of K (*i.e.*, the minimum centrifugal barrier) satisfying the symmetry requirements, express the minimum-energy J^P configuration coming out from our dynamical model.

It is worth to mention that the same spectral patterns and rules could be also derived from a careful look at data in order to apply a general quark model multiplet structure as done in ref. [16]. However, in this case the lack of an underlying dynamics prevents, as pointed by the author, a justification for the phenomenological rules derived.

3.2 Positive-parity states

For positive-parity states the emerging picture consists of two sets (spatially symmetric and mixed corresponding to the upper and lower parts of table 3, respectively) of N's and Δ's grouped according to the same dominant configurations. Each Δ state, except for the $\Delta(1/2^+)$, has a nucleon correspondence. For $\Delta(1/2^+)$ its *natural* nucleon partner should be a $N(3/2^+)$ with $(L=0,S=3/2)$ which, as mentioned above, is dynamically unfavored. Actually, our model predicts for $N(3/2^+)$ $(L=2,S=1/2)$ a lower mass than for $\Delta(1/2^+)$ as it is the experimental case.

It is important to realize that the percentage of the dominant configuration in the sets varies: while for the upper part it can be quite different for N and Δ partners (for example, 62% of $(2,2,[3])$ for $N(5/2^+)$ and 99% for $\Delta(7/2^+)$), for the lower part it is quite approximately the same and very close to 100% (for instance, 99% of $(2,2,[21])$ for $\Delta(5/2^+)$ and 99% for $N(7/2^+)$). This has to do with the fact that for the lower-part series only a spatially mixed wave function is allowed, whereas for the upper-part N series there are, except for $N(1/2^+)$, two possibilities open for the same (K,L) values: spatially symmetric (spin-isospin symmetric) and spatially mixed (spin-isospin mixed).

For the upper-part set, the lowest-lying states, $N(1/2^+)$ and $\Delta(3/2^+)$, with a dominant configuration $(0,0,[3])$, have an energy difference of 292 MeV, entirely due in our model to the spin-spin potential, attractive for $S=1/2$ and repulsive for $S=3/2$, since for both states the percentage of the dominant configuration is almost the same (98% for $N(1/2^+)$ and 100% for $\Delta(3/2^+)$). Let us keep in mind that *chiral* contributions from meson exchanges are taken into account through the effective quark-gluon coupling constant fitted to the $\Delta(3/2^+)-N(1/2^+)$ mass difference. For the next dominant configuration, containing the $N(5/2^+)$ and the $\Delta(7/2^+)$, whose masses are quite well reproduced by our model, one has to consider the configuration mixing effect in $N(5/2^+)$ (62% of $(2,2,[3])$ and 34% of $(2,2,[21])$). Let us realize though that both configurations would give the same energy for an hypercentral (only ρ-dependent) potential. As our (confinement + Coulomb) potential is quite close to an hypercentral one, the difference between N and Δ partners is again due in our model to the spin-spin interaction. We predict 199 MeV. This means

Table 3. Positive-parity N and Δ ground states for different dominant spatial-spin configurations up to $\simeq 3\,\mathrm{GeV}$. The assignment of dominant configurations above 2.4 GeV corresponds to an educated guess. Experimental data are from PDG [13]. Stars have been omitted for four-star resonances. States denoted by a question mark correspond to predicted resonances that do not appear in the PDG (their predicted masses, also indicated by a question mark, appear in table 7).

$(K, L, Symmetry)$	$S = 1/2$	Model (MeV)		Exp. (MeV)		$S = 3/2$
$(0, 0, [3])$	$N(1/2^+)$	940		940		
			1232		1232	$\Delta(3/2^+)$
$(2, 2, [3])$	$N(5/2^+), N(3/2^+)$	1722		1680,1720		
			1921		1950	$\Delta(7/2^+)$
$(4, 4, [3])$	$N(9/2^+)$	2378		2220		
			2175		2420	$\Delta(11/2^+)$
$(6, 6, [3])$	$N(13/2^+)(**)$			2700		
					2950	$\Delta(15/2^+)(**)$
$(2, 0, [21])$	$\Delta(1/2^+)$		1849		1750	
$(2, 2, [21])$		1938		1990		$N(7/2^+)(**)$
	$\Delta(5/2^+)$		1871		1905	
$(4, 4, [21])$				?		$N(11/2^+)(?)$
	$\Delta(9/2^+)(**)$		2193		2300	
$(6, 6, [21])$				?		$N(15/2^+)(?)$
	$\Delta(13/2^+)(?)$				?	

Table 4. Negative-parity N and Δ ground states for different dominant spatial-spin configurations up to $\simeq 3\,\mathrm{GeV}$. The assignment of dominant configurations above 2.4 GeV correspond to an educated guess. Experimental data are from PDG [13]. Stars have been omitted for four-star resonances. States denoted by a question mark correspond to predicted resonances that do not appear in the PDG (their predicted masses, also indicated by a question mark, appear in table 7).

$(K, L, Symmetry)$	$S = 1/2$	Model (MeV)		Exp. (MeV)		$S = 3/2$
$(1, 1, [21])$	$N(3/2^-), N(1/2^-)$	1410		1520,1535		
		1596		1675		$N(5/2^-)$
	$\Delta(3/2^-), \Delta(1/2^-)$		1517		1700,1620	
$(3, 3, [21])$	$N(7/2^-)$	2275		2190		
		2153		2250		$N(9/2^-)$
	$\Delta(7/2^-)(*)$		2153		2200	
$(5, 5, [21])$	$N(11/2^-)(***)$			2600		
				?		$N(13/2^-)(?)$
	$\Delta(11/2^-)(?)$				?	
$(3, 1, [3])$			2114		1930	$\Delta(5/2^-)(***)$
$(5, 3, [3])$			2153		2400	$\Delta(9/2^-)(**)$
$(7, 5, [3])$					2750	$\Delta(13/2^-)(**)$

a slow variation of the spin-spin contribution when increasing K and L for spatially symmetric states (actually the 62% of the $\Delta(3/2^+) - N(1/2^+)$ mass difference is 181 MeV). The experimental $\Delta - N$ energy difference is bigger, $\Delta(7/2^+) - N(5/2^+) \simeq 270\,\mathrm{MeV}$, but also seem to vary slowly: $\Delta(11/2^+) - N(9/2^+) \simeq 200\,\mathrm{MeV}$, $\Delta(15/2^+) - N(13/2^+) \simeq 250\,\mathrm{MeV}$. This may be reflecting a larger probability for the spatially symmetric component than given by our model (let us point in addition that the more cumbersome numerical procedure for $J \geq 9/2$ states due to the presence of thresholds, makes less accurate our predictions, indeed the calculated energies for $N(9/2^+)$ and $\Delta(11/2^+)$ are inverted with respect to data). These quantitative differences should be expected given the shortcomings of our dynamical model. However, the spectral pattern derived is very useful to make manifest a regularity in the data: the experimental N and Δ energy steps when going from one dominant configuration to the next one remain also constant about 500 MeV: $N(9/2^+) - N(5/2^+) \simeq 540\,\mathrm{MeV}$, $\Delta(11/2^+) - \Delta(7/2^+) \simeq 470\,\mathrm{MeV}$, $N(13/2^+) - N(9/2^+) \simeq 480\,\mathrm{MeV}$, $\Delta(15/2^+) - \Delta(11/2^+) \simeq 530\,\mathrm{MeV}$ (this energy step can be associated, from our model, to $\Delta K = \Delta L = 2$). The extension of this pattern to further steps allows us to pre-

dict that a $N(17/2^+)$, if existing identifiable experimental resonances at such high energies, would have a mass of 3200 MeV.

Regarding the lower-part set we should notice that the same configuration percentage for N's and Δ's would imply a degeneracy, term by term, if only spatial (neither spin- nor isospin-dependent) interactions were considered, $N(7/2^+) : \Delta(5/2^+)$; $N(11/2^+) : \Delta(9/2^+)$, ... As a matter of fact, as for this set the spin-spin interaction (the only nonspatial one in our model) gives little contribution, due to its short-range character and the spatial mixed symmetry involved (with $K = L \geq 2$), the difference between the $N(7/2^+)$ and $\Delta(5/2^+)$ masses (the only states clearly below threshold) is in our model less than 5%, what seems to be corroborated by data (this could be an indication that isospin-dependent interactions do not contribute significantly as well). Concerning the energy step, we expect from our analysis above ($\Delta K = \Delta L = 2$) and the scarce data ($\Delta(9/2^+) - \Delta(5/2^+) \simeq 400$ MeV) an approximate constant value around 400–500 MeV. From this there would appear a $N(11/2^+)$ at about 2450 MeV (the energy of its two stars $\Delta(9/2^+)$ partner is experimentally in the interval 2200–2500 MeV), a $\Delta(13/2^+)$ and a $N(15/2^+)$ at about 2900 MeV and a $\Delta(17/2^+)$ around 3300 MeV.

All predictions of our model up to 3 GeV, from this subsection and next subsections (3.3 and 3.5), are summed up in table 7.

3.3 Negative-parity states

For negative-parity states the results are organized in table 4. The upper part corresponds to spatially mixed configurations for which we expect, from our model, a rapid decrement in the spin-spin energy difference between N and Δ partners when going from $K = L = 1$ to $K = L \geq 3$ and, as a consequence, all the states with the same dominant configuration should become close in mass. The data seem to follow this prescription: mass differences of 180 MeV at most for $K = L = 1$, 60 MeV for $K = L = 3, \ldots$. Again the spectral pattern makes manifest the energy step (400–500 MeV) regularity in the data: ($N(9/2^-) - N(5/2^-) = 575$ MeV; $\Delta(7/2^-) - \Delta(3/2^-) = 500$ MeV, $N(11/2^-) - N(7/2^-) = 410$ MeV) as it corresponds to $\Delta K = \Delta L = 2$. Therefore, one would expect a $N(13/2^-)$ and a $\Delta(11/2^-)$ at about 2650 MeV and a $N(15/2^-)$, a $\Delta(15/2^-)$ and a $N(17/2^-)$ at about 3050 MeV.

The lower part of table 4 contains an independent series of Δ's without N's partners. All states are above their lowest threshold. From the analysis above we can expect again a step energy, corresponding to $\Delta K = \Delta L = 2$, of around 400–500 MeV that turns out to be compatible with data within the experimental errors. From this a $\Delta(17/2^-)$ would be located at approximately 3200 MeV.

3.4 N − Δ approximate degeneracies

According to our model, the masses of the $N(J^-)$ and $\Delta(J^-)$ in the left-hand side of table 4 should become degenerate as the effective spin-spin interaction becomes weaker and the potential approaches an hypercentral one. This seems also to be the experimental situation.

Table 5. N and Δ approximate degeneracies up to $\simeq 3$ GeV. Experimental masses (in MeV) from PDG [13]. Predicted masses are signaled by a question mark.

N		Δ
$N(7/2^-)(2190)$	:	$\Delta(7/2^-)(2200)$
$N(11/2^-)(2600)$	:	$\Delta(11/2^-)(2650?)$
$N(7/2^+)(1990)$	:	$\Delta(7/2^+)(1950)$
$N(11/2^+)(2450?)$	:	$\Delta(11/2^+)(2420)$
$N(15/2^+)(2900?)$	:	$\Delta(15/2^+)(2950)$

On the other hand, the $N(J^+)$ and $\Delta(J^+)$ on the right-hand side of table 3 should become degenerate as the spin-spin contribution for $S = 3/2$ (significantly smaller than for $S = 1/2$ in spatially symmetric states) is not quantitatively much different for spatially symmetric and mixed states. This is confirmed by the scarce data available ($J^P = 7/2^+$).

These results, from data and our predictions, are picked up in table 5. We can express its content in a schematic simplified manner through:

$$N(J^{+,-}) \simeq \Delta(J^{+,-}) \qquad \text{for} \qquad J = \frac{4n+3}{2} \qquad \text{with} \qquad n = 1, 2, 3, \ldots . \tag{7}$$

Let us realize that for positive-parity eq. (7) corresponds to a rule derived in ref. [16] from a phenomenological mass formula obtained from the assumption of linear Regge trajectories.

3.5 Excited states

For excited states in general the situation is much more cumbersome. Though both models, smooth and sharp, provide a similar pattern a more careful analysis of the configurations entering the states makes clear significant differences. For instance, the fourth $N(1/2^+)$ state has for the smooth potential a $(2, 2, [21]), S = 3/2$ component degenerate (at the level of precision of the model) with the $(2, 1, [111])$, $S = 1/2$, while the same state corresponds uniquely to the last configuration for the sharp potential. For $\Delta(3/2^+)$ in the sharp case, the radial excitation of $(0, 0, [3]), S = 3/2$ and the $(2, 2, [21]), S = 1/2$ configurations are degenerate, whereas in the smooth case, the radial excitation of $(0, 0, [3]), S = 3/2$ is the first excited state and it is not degenerate, etc. Moreover, the first radial excitations of $\Delta(3/2^+)$ at 1600 MeV and $N(1/2^+)$ at 1440 MeV are badly predicted. In contrast to this inadequacy to deal with the radial excitations and the strong model dependence of the configurations for higher (second and up) excitations, our dynamics provides a very simple picture for the first non-radial excitations that follows the

Table 6. Ground and first nonradial excitation (denoted by a black dot) correspondence according to our model up to $\simeq 3\,\mathrm{GeV}$. Experimental masses (in MeV) from PDG [13]. Experimental unknown masses are signaled by a question mark.

N			Δ		
			$\Delta(3/2^+)^\bullet(1920)$	:	$\Delta(5/2^+)(1905)$
$N(5/2^+)^\bullet(2000)$	:	$N(7/2^+)(1990)$	$\Delta(5/2^+)^\bullet(2000)$	:	$\Delta(7/2^+)(1950)$
$N(7/2^+)^\bullet(?)$	:	$N(9/2^+)(2220)$	$\Delta(7/2^+)^\bullet(2390)$	:	$\Delta(9/2^+)(2300)$
$N(9/2^+)^\bullet(?)$	:	$N(11/2^+)(?)$	$\Delta(9/2^+)^\bullet(?)$	:	$\Delta(11/2^+)(2420)$
$N(11/2^+)^\bullet(?)$	:	$N(13/2^+)(2700)$	$\Delta(11/2^+)^\bullet(?)$	:	$\Delta(13/2^+)(?)$
$N(13/2^+)^\bullet(?)$	:	$N(15/2^+)(?)$	$\Delta(13/2^+)^\bullet(?)$	:	$\Delta(15/2^+)(2950)$
$N(3/2^-)^\bullet(1700)$	:	$N(5/2^-)(1675)$			
$N(5/2^-)^\bullet(2200)$	:	$N(7/2^-)(2190)$	$\Delta(5/2^-)^\bullet(2350)$	:	$\Delta(7/2^-)(2200)$
$N(7/2^-)^\bullet(?)$	:	$N(9/2^-)(2250)$	$\Delta(7/2^-)^\bullet(?)$	:	$\Delta(9/2^-)(2400)$
$N(9/2^-)^\bullet(?)$	:	$N(11/2^-)(2600)$	$\Delta(9/2^-)^\bullet(?)$	:	$\Delta(11/2^-)(?)$
$N(11/2^-)^\bullet(?)$	:	$N(13/2^-)(?)$	$\Delta(11/2^-)^\bullet(?)$	:	$\Delta(13/2^-)(2750)$

Table 7. N and Δ predicted states in the interval $[2.2, 3.0]\,\mathrm{MeV}$. We denote by a black dot the first nonradial excitation.

	N		Δ	
$J = 7/2$	$N(7/2^+)^\bullet(2220)$	$N(7/2^-)^\bullet(2250)$		$\Delta(7/2^-)^\bullet(2400)$
$J = 9/2$	$N(9/2^+)^\bullet(2450)$	$N(9/2^-)^\bullet(2600)$	$\Delta(9/2^+)^\bullet(2420)$	$\Delta(9/2^-)^\bullet(2650)$
$J = 11/2$	$N(11/2^+)(2450)$			$\Delta(11/2^-)(2650)$
	$N(11/2^+)^\bullet(2700)$	$N(11/2^-)^\bullet(2650)$	$\Delta(11/2^+)^\bullet(2900)$	$\Delta(11/2^-)^\bullet(2750)$
$J = 13/2$		$N(13/2^-)(2650)$	$\Delta(13/2^+)(2900)$	
	$N(13/2^+)^\bullet(2900)$		$\Delta(13/2^+)^\bullet(2950)$	
$J = 15/2$	$N(15/2^+)(2900)$			

trend of data. The rule, coming from the absence of spin-orbit and tensor forces in our model, and again of general validity for $J \geq 5/2$, is:

The first non-radial excitation of $N, \Delta(J)$ *and the ground state of* $N, \Delta(J+1)$ *respectively, are almost degenerate.* (8)

This rule is satisfied by existing data at the level of 3%, table 6. From now on we will denote by a black dot the first nonradial excitation of any state. The only significant deviation from the previous rule, $\Delta(5/2^-)^\bullet(2350) : \Delta(7/2^-)(2200)$ (7% of difference), corresponds to two resonances catalogued as one star by the PDG. Indeed, the degeneracy can be accomplished within the experimental uncertainties, see fig. 5.

Assuming this approximate degeneracy we can guess, from data and from our phenomenological ground-state predictions above, the masses for the first nonradial excited states with a question mark in table 6. These predictions, up to $\simeq 3\,\mathrm{GeV}$, are summed up in table 7.

For $J < 5/2$ the rule is only satisfied, according to our model, by $N(3/2^-)$ and $\Delta(3/2^+)$. For some of the remaining states our model gives also definite relations between their first nonradial excitations and other ground or excited states. These relations are quite reasonably satisfied by the data too: $N(1/2^-)^\bullet(1650) : N(3/2^-)^\bullet(1700) : N(5/2^-)(1675)$, $\Delta(1/2^-)^\bullet(1900) : \Delta(3/2^-)^\bullet(1940)$, $\Delta(1/2^+)^\bullet(1910) : \Delta(5/2^+)^\bullet(2000) : \Delta(7/2^+)(1950)$.

It is worth to remark that some of our findings in table 7 might be in fact already accomplished by current data although being masked by the experimental uncertainties (see figs. 4 and 5). For example, the $N(7/2^{+,-})^\bullet$ could be, within theoretical plus experimental errors, in the $N(7/2^{+,-})$, the $\Delta(7/2^-)^\bullet$ in the $\Delta(7/2^-)$ and so on. We should also realize that some of the predicted resonances could have small couplings to formation channels, what would make difficult its detection (see, for example, ref. [6] regarding $N(11/2^+)$, $N(13/2^-)$ and $N(15/2^+)$).

3.6 Parity series

A look at tables 3, 4 and 7 shows some approximate $N(J^P)$ parity doublets. Thus, for $J \geq 5/2$ the N^+ ground-state series in the upper part of table 3 and the N^- ground-state series in the upper part of table 4 appear almost degenerate, term by term, for example $N(5/2^+)(1680) : N(5/2^-)(1675)$, as shown on the left-hand side of table 8. From our model we can propose a qualitative systematic for this doubling: the bigger repulsion in the positive-parity state with respect to the negative-parity one, due to $\Delta K = 1, \Delta L = 1$, is compensated by the bigger attraction in a spatially symmetric $S = 1/2$ configuration (*i.e.*, $\Delta S = -1$). We can quantify

Table 8. Dynamical parity doublets from our analysis up to $\simeq 3\,\mathrm{GeV}$. Experimental masses (in MeV) from PDG [13]. Predicted masses are signaled by a question mark. The black dot indicates the first nonradial excitation.

N	
Ground states	First nonradial excitation
$N(5/2^+)(1680)$: $N(5/2^-)(1675)$	$N(7/2^+)^\bullet(2220?)$: $N(7/2^-)^\bullet(2250?)$
$N(9/2^+)(2220)$: $N(9/2^-)(2250)$	$N(11/2^+)^\bullet(2700?)$: $N(11/2^-)^\bullet(2650?)$
$N(13/2^+)(2700)$: $N(13/2^-)(2650?)$	

these effects from our data analysis above. We can estimate an increment of the repulsion energy of $\simeq 250\,\mathrm{MeV}$ (from $\simeq 500\,\mathrm{MeV}$ for $\Delta K = 2$, $\Delta L = 2$, as previously discussed) and an increment in the attraction, when going from $S = 3/2$ to $S = 1/2$ of approximately the same amount. So we can predict further parity doublings, $N(13/2^+) : N(13/2^-)$, ... Moreover, the application of our preceding rules for the first non-radial excitations gives rise to an equivalent approximate parity doublet series, right-hand side of table 8.

For Δ's ($J \geq 5/2$) although an inspection to data in tables 3 and 4 might also suggest some approximate degeneracies: the $\Delta(J^{+,-})$ ground-state series in the lower parts of table 3 and table 4 could be almost degenerate, term by term: $\Delta(5/2^+)(1905) : \Delta(5/2^-)(1930)$, $\Delta(9/2^+)(2300) : \Delta(9/2^-)(2400), \ldots$, we expect our model not to support this suggestion. Indeed going from the positive to the corresponding negative-parity state we expect the centrifugal repulsion getting increased ($\Delta K = 1$) and the spin-spin interaction changing from attractive ($S = 1/2$) to repulsive ($S = 3/2$), hence the J^- states should be higher in mass than the J^+ ones.

We should realize that the approximate N parity doublets appear discretely, every 500 MeV. This does not preclude the existence for other energies of additional (N and/or Δ) parity doublets involving higher excitations but we cannot carry out for them a trustable analysis.

4 Summary

We have performed a phenomenological analysis of the nonstrange-baryon spectrum between 2.3 and 3 GeV. Our starting point is a quark model potential, containing confinement and OGE interactions saturating at 2.4 GeV, that gives the correct number and ordering of known resonances up to 2.3 GeV. The study of the dominant configurations entering the ground state and the first nonradial excitations provides us with quantum number spectral patterns. The extrapolation of these patterns to higher energies allows the prediction, from existing data, of ground ($J \geq 11/2$) and first nonradial excited ($J \geq 7/2$) state masses in the quite experimentally uncertain energy region from 2.3 to 3 GeV. It is precisely this uncertainty, reflecting the transition to the continuum, what makes our picture plausible despite the blown up number of *new* states.

The qualitative adequacy of our model description to data suggests that the effective (confinement + Coulomb + spin-spin) dynamics employed (we have estimated numerically small contributions of conventional meson exchange potentials to the mass of $J \geq 5/2$ baryons) contains the essential ingredients to give account of the observed regularities in the spectrum. In this respect, we should emphasize i) the usefulness of screening as an effective mechanism in quark potential models to provide an unambiguous assignment of quantum numbers to states (this is related to the connection of screening to decay channel effects as shown by lattice calculations) and ii) the importance of using the hyperspherical harmonic basis as the more convenient to deal, from the point of view of the physical interpretation, with the quasi-hypercentral potential considered.

From data and our predictions we find, on the one hand, approximate $N - \Delta$ degeneracies and, on the other hand, series of N parity doublets involving ground or first nonradial excitations exclusively. We get from our minimal dynamics some understanding about how these degeneracies come out.

We should finally remark that our results do not rely on any symmetry assumption in QCD, but on a particular dynamics that provides a spectral pattern in agreement to data. Since existing data beyond 1.9 GeV are plagued with large experimental errors, we cannot pretend our quantitative predictions to be very precise. Nonetheless, we think our findings can be of help for the always needed experimental spectral searches in this region as well as for the theoretical progress in the dynamical interpretation of data.

This work has been partially funded by Ministerio de Ciencia y Tecnología under Contract No. FPA2004-05616, by Junta de Castilla y León under Contract No. SA-104/04, and by Generalitat Valenciana under Contract No. GV05/276.

References

1. G.S. Bali, Phys. Rep. **343**, 1 (2001).
2. SESAM Collaboration (G.S. Bali, H. Neff, T. Düssel, T. Lippert, K. Schilling), Phys. Rev. D **71**, 114513 (2005).
3. D. Jido, T. Hatsuda, T. Kunihiro, Phys. Rev. Lett. **84**, 3252 (2000); D. Jido, M. Oka, A. Hosaka, Prog. Theor. Phys. **106**, 873 (2001); T.D. Cohen, L.Ya. Glozman, Phys. Rev. D **65**, 016006 (2002); Int. J. Mod. Phys. A **17**, 1327 (2002).

4. R.L. Jaffe, D. Pirjol, A. Scardicchio, Phys. Rev. Lett. **96** 121601 (2006); hep-ph/0602010.
5. S. Capstick, W. Roberts, Prog. Part. Nucl. Phys. **45**, S241 (2000) and references therein.
6. S. Capstick, W. Roberts, Phys. Rev. D **47**, 1994 (1993).
7. J. Vijande, P. González, H. Garcilazo, A. Valcarce, Phys. Rev. D **69**, 074019 (2004).
8. K.D. Born, E. Laermann, N. Pirch, T.F. Walsh, P.M. Zerwas, Phys. Rev. D **40**, 1653 (1989).
9. Z. Zhang, Y. Yu, P. Shen, X. Shen, Y. Dong, Nucl. Phys. A **561**, 595 (1993).
10. Y.B. Ding, K.T. Chao, D.H. Qin, Phys. Rev. D **51**, 5064 (1995).
11. M.M. Brisudová, L. Burakovsky, T. Goldman, Phys. Rev. D **61**, 054013 (2000).
12. P. González, A. Valcarce, H. Garcilazo, J. Vijande, Phys. Rev. D **68**, 034007 (2003).
13. S. Eidelman *et al.*, Phys. Lett. B **592**, 1 (2004).
14. E.S. Swanson, J. Phys. G **31**, 845 (2005).
15. P. González, A. Valcarce, J. Vijande, H. Garcilazo, Int. J. Mod. Phys. A **20**, 1842 (2005).
16. E. Klempt, Phys. Rev. C **66**, 058201 (2002).